Journal of the Taiwan Institute of Chemical Engineers 93 (2018) 477–484

Contents lists available at ScienceDirect

Journal of the Taiwan Institute of Chemical Engineers

journal homepage: www.elsevier.com/locate/jtice

Nano-engineered hexagonal PtCuCo nanocrystals with enhanced catalytic activity for ethylene glycol and glycerol electrooxidation

Chunyang Zhai[a], Jiayue Hu[a], Haifeng Gao[a], Lixi Zeng[b,*], Mianqiang Xue[c,*], Zhao-Qing Liu[d], Mingshan Zhu[b,*]

[a] School of Materials Science and Chemical Engineering, Ningbo University, Ningbo 315211, PR China
[b] Guangdong Key Laboratory of Environmental Pollution and Health, School of Environment, Jinan University, Guangzhou 510632, PR China
[c] Research Institute of Science for Safety and Sustainability, National Institute of Advanced Industrial Science and Technology, Ibaraki 305-8569, Japan
[d] School of Chemistry and Chemical Engineering, Guangzhou University, Guangzhou, 510006, PR China

ARTICLE INFO

Article history:
Received 10 June 2018
Revised 10 August 2018
Accepted 10 August 2018
Available online 5 September 2018

Keywords:
Trimetallic nanocatalysts
Rational design
Hexagonal nanocrystals
Fuel cells

ABSTRACT

Although great advances have been achieved in the field of fuel cells, the lack of cost-efficient electrocatalysts is still the grand challenge impeding the practical application of fuel cells. To this end, rational design of efficient multicomponent electrocatalysts with both high activity and stability is highly momentous for fuel cell reaction. Herein, a facile approach to controllably engineer trimetallic hexagonal PtCuCo nanocrystals (NCs) as highly active and durable liquid fuel electrooxidation catalysts is reported. Impressively, after the incorporation of Cu and Co into Pt, the electronic structures of Pt remarkably modified, leading to the enhancement of electrocatalytic performances. The optimized hexagonal PtCuCo NCs were demonstrated to display outstanding activities of 4926.4 and 3519.9 mA mg^{-1} for the electrooxidation of ethylene glycol (EG) and glycerol, in comparison with Pt/C catalysts. The greatly improved activity of hexagonal PtCuCo NCs is ascribed to the highly exposed surface active areas and the electronic effects among Pt, Cu, and Co. More importantly, the trimetallic hexagonal nanocatalysts also display great durability with little variations in composition, structure, and activity, showing an advanced class of nanocatalysts for fuel cells and beyond.

1. Introduction

The rational fabrication and development of advanced technologies for highly efficient energy conversion devices is attractive to relieve energy crisis [1–3]. In numerous innovative strategies, direct fuel cells, with the features of high efficiency, clean, and environmental friendliness, show great promise as ideal technologies for the transition to a hydrogen based economy [4–6]. Unfortunately, some drawbacks related to the electrocatalysts such as high cost, sluggish reaction kinetics, and poor durability have severely hindered their practical application [7–9]. To this end, intensive efforts have been devoted to the construction of ideal electrocatalysts with both high activity and durability. As the most promising catalyst for fuel cells reaction, noble-metal Pt material has attracted massive research attentions over decades, while its exorbitant price and scarcity have limited its future development in fuel cells [10–12]. To this end, improving Pt utilization is demonstrated to be an efficient approach for promoting their intrinsic activity and durability, which is meaningful for the development of fuel cells technology.

Regarding improving Pt utilization, many strategies have been developed. Among them, alloying Pt with other earth-abundant metals has been generally regarded as a feasible method [13–15]. On one hand, the incorporation of earth-abundant metals can reduce the cost of electrocatalysts, on the other hand, benefitting for the synergistic and electronic effects, the newly-generated Pt-based multicomponent nanocatalysts can display greatly enhanced electrocatalytic performances [16–18]. In addition, the introduction of other metals is also favorable for breaking the C–C bonds of alcohol molecules during the oxidation reaction. More importantly, after the incorporation of other metals, the d-band center of Pt will downshift [19,20], which thus promote of catalytic performances to a higher level.

Besides the compositions, the electrocatalytic performances of Pt or Pt-based nanocatalysts also greatly rely on their structures since the electrocatalytic reaction usually takes place on the surface of catalyst, and the nanocatalysts with unique morphology can expose highly active facets and abundant surface active sites [21–23]. Accordingly, multicomponent Pt-based catalysts with fascinating nanostructures such as hollow [24,25], nanowire [26],

* Corresponding authors.
E-mail addresses: lxzeng@jnu.edu.cn (L. Zeng), mq_xue@yahoo.com (M. Xue), mingshanzhu@yahoo.com (M. Zhu).

https://doi.org/10.1016/j.jtice.2018.08.023
1876-1070/

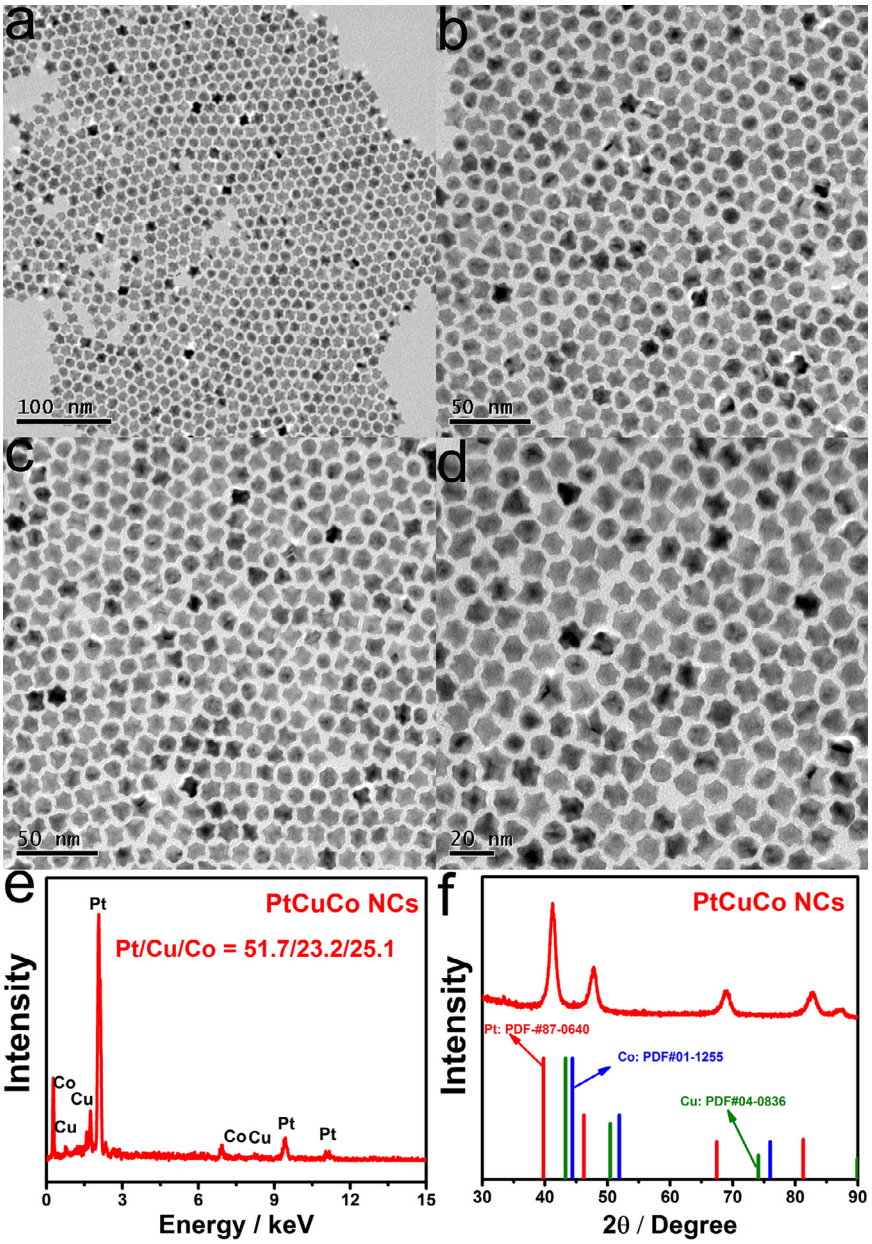

Fig. 1. (a–d) The TEM images of hexagonal PtCuCo NCs with different magnifications. (e) SEM–EDX and (f) PXRD patterns of PtCuCo NCs.

and dendrite [27] have been well designed and engineered. And the electrochemical measurements have revealed that well-defined nanocatalysts bounded with high surface areas possess substantial enhancement in both catalytic activity and stability [28,29]. Among them, the hexagonal nanostructure with abundant surface active areas is attractive to greatly enhance the electrocatalytic activity because of its abundant kinks, ledges, and atomic steps on the surface [30].

Aiming to achieve cost-efficient multicomponent Pt-based nanocatalysts and boost the commercial development of fuel cells, here we report the successful design of fascinating hexagonal PtCuCo nanostructures in the mild reaction conditions. Abundant atomic steps, ledges, and kinks on the surface of hexagonal nanostructures help the PtCuCo nanocatalysts expose more active sites for EG and glycerol molecules. Impressively, it was demonstrated that the as-obtained trimetallic PtCuCo hexagonal NCs could exhibit unexpectedly high catalytic property towards EG oxidation reaction (EGOR) and glycerol oxidation reaction (GOR), with the mass activities found to be 4926.4 and 3519.9 mA mg^{-1}, which are 4.2 and 4.9 times greater than those of Pt/C catalysts. More significantly, the long-term electrochemical tests have also demonstrated its outstanding durability with extremely high retained activity, showing a variety of promising well-defined electrocatalysts for fuel cells.

2. Experimental section

2.1. Preparation of hexagonal PtCuCo NCs

The hexagonal PtCuCo NCs were prepared according to a milder wet-chemical method similar to previous method [31]. In the standard synthesis of hexagonal PtCuCo NCs, 10 mg $Pt(acac)_2$, 2.1 mg $CuCl_2{\cdot}2H_2O$, 3.4 mg $Co(acac)_2$, 36.5 mg hexadecyltrimethylammonium bromide (CTAB, 99%), 7 mL oleylamine (OAm, $CH_3(CH_2)_7CH=CH(CH_2)_7CH_2NH_2$, 70%), and 2 mL octadecylene (ODE, >98.0%) were added to a vial (volume: 30 mL). After

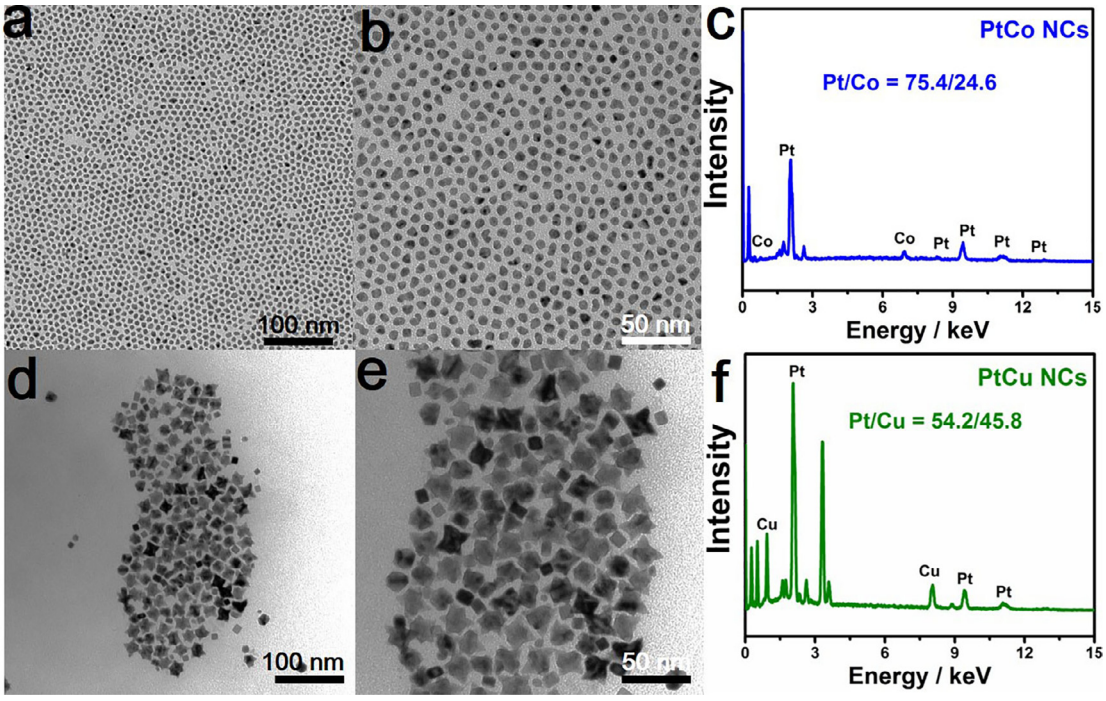

Fig. 2. (a and b) TEM images of PtCo NCs and (c) their SEM–EDX patterns. (d and e) TEM images of PtCu NCs and (f) their SEM–EDX patterns.

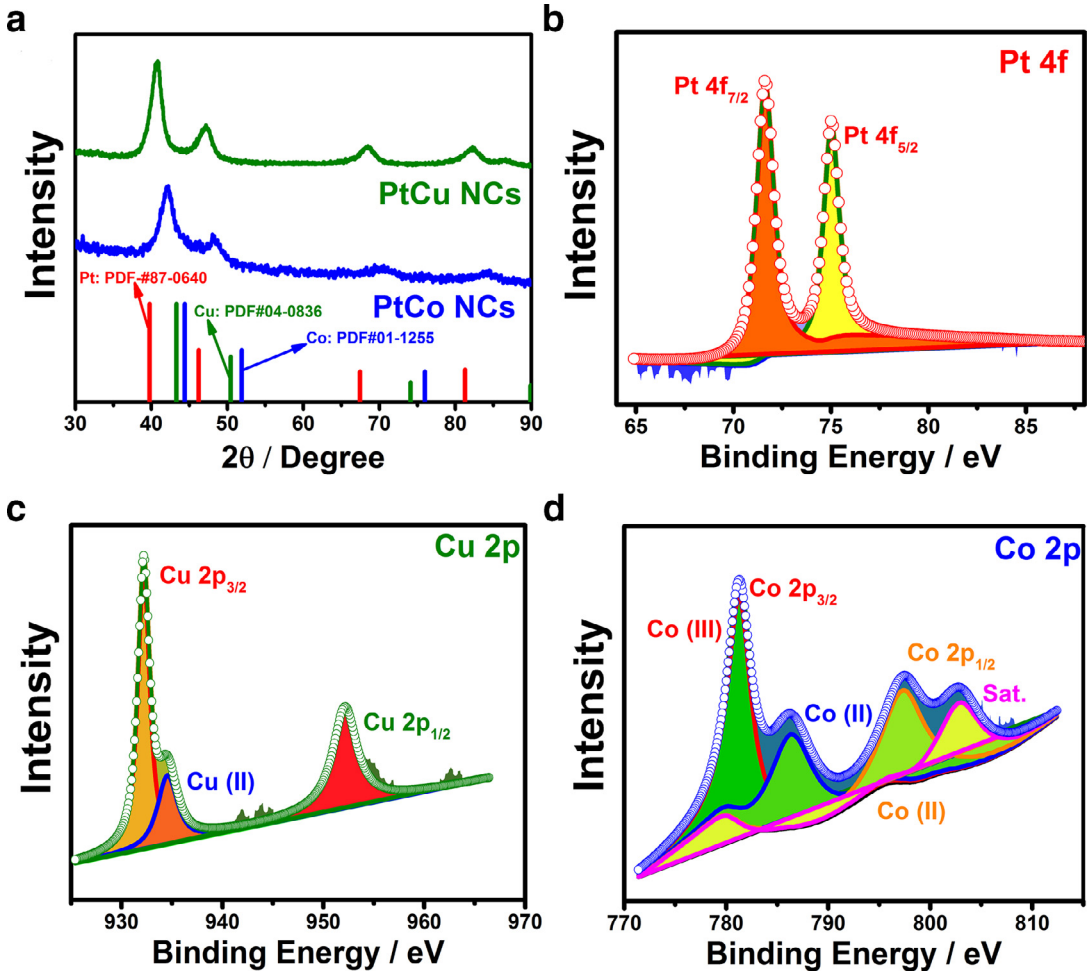

Fig. 3. (a) PXRD patterns of PtCu and PtCo NCs. (b) XPS spectra of (b) Pt 4f, (c) Cu 2p, and (d) Co 2p.

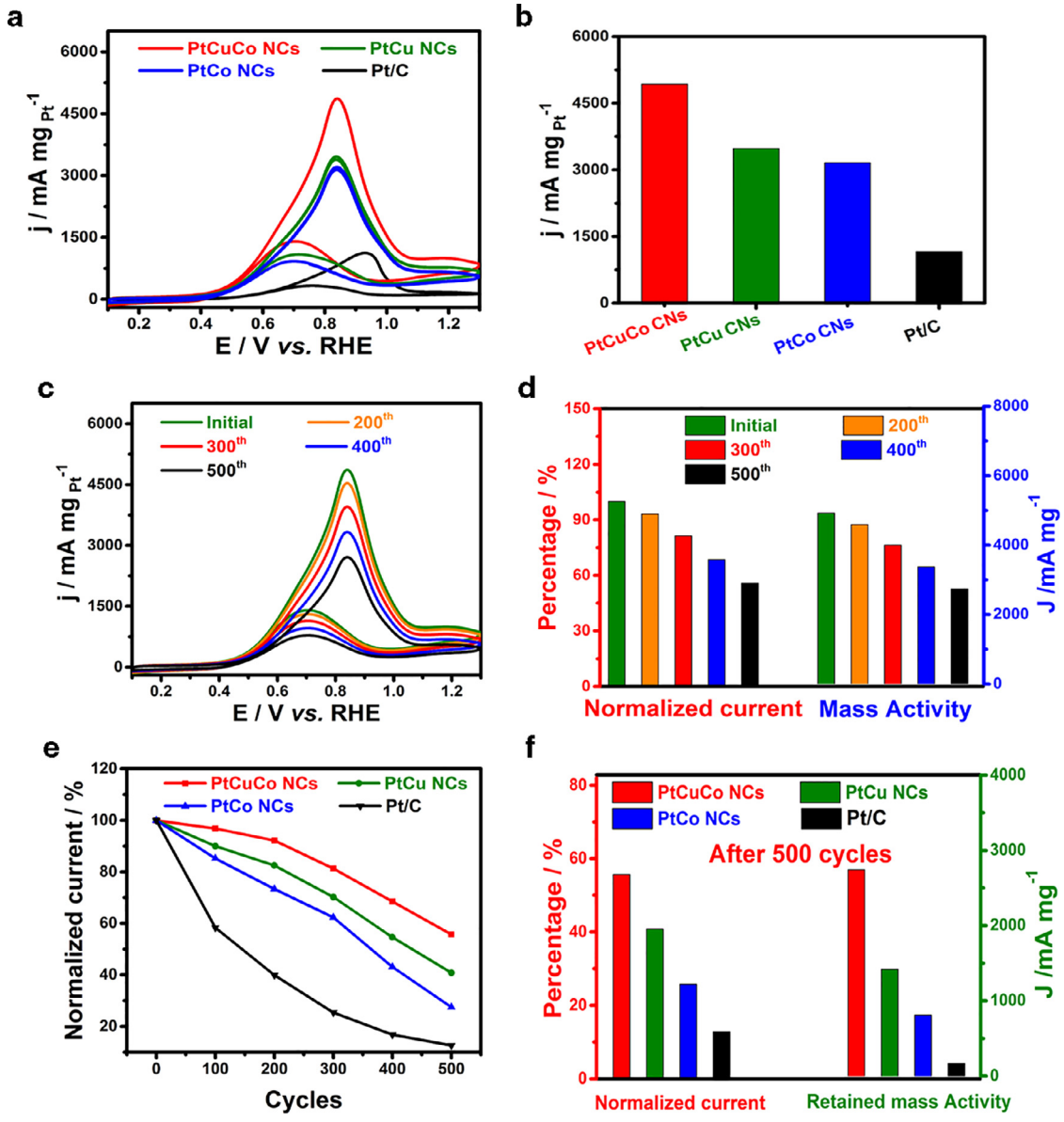

Fig. 4. (a) CV curves of PtCuCo, PtCu, and PtCo NCs, as well as Pt/C catalysts towards EGOR at the scan rate of 50 mV s^{-1}. (b) The corresponding histogram of mass activities of these electrocatalysts. (c) Initial, 200th, 300th, 400th, and 500th CV curves of PtCuCo towards EGOR and (d) its corresponding histogram of normalized current percentage and retained mass activities. (e) Durability comparison of PtCuCo, PtCu, and PtCo NCs, as well as Pt/C catalysts towards EGOR and its corresponding histogram of normalized current percentage and retained mass activities.

the vial has been capped, the mixture was then ultrasonicated for 30 min. The vial was then transferred to an oil bath to heat form room temperature to 200 °C for another 5 h. The resulting products could be collected by centrifugation (10,000 rpm) and washed with ethanol/cyclohexane mixture. The syntheses of PtCu and PtCo NCs were similar to hexagonal PtCuCo NCs except for the addition of $Co(acac)_2$ and $CuCl_2{\cdot}2H_2O$, respectively.

2.2. Characterization

The compositions of the catalysts before and after electrochemical measurements were determined by the inductively coupled plasma atomic emission spectroscopy (ICP-AES, 710-ES, Varian). The morphologies and sizes of samples were determined by transmission electron microscope (TEM) (Tecnai G220, FEI America) at 200 kV. And the samples were prepared by dropping ethanol dispersion of products onto carbon-coated copper TEM grids using pipettes. The SEM energy dispersive X-ray (EDX) images were taken with a HITACHI S-3700 cold field emission scanning electron microscope operated at 15 kV. The powder X-ray diffraction (PXRD) patterns were collected using an X'Pert-Pro X-ray powder diffractometer equipped with a Cu radiation source ($\lambda = 0.15406$ nm). X-ray photoelectron spectroscopy (XPS) was conducted on a Thermo Scientific ESCALAB 250 XI X-ray photoelectron spectrometer.

2.3. Electrochemical measurements

For the typical electrocatalytic reaction, a standard three-electrode cell was used for performing all the tests. Before the electrochemical measurement, we loaded the catalysts on carbon black (Vulcan XC72R carbon, C) by sonication and washed with acetic acid at room temperature twice. To prepare a catalyst-coated working electrode, the catalyst was dispersed in a mixture of solvents containing isopropanol and Nafion (5%) to form a 0.20 mg_{Pt} mL^{-1} suspension. A 10 μL isopropanol dispersion of samples on carbon (0.20 mg_{Pt} mL^{-1}) was deposited on a glassy

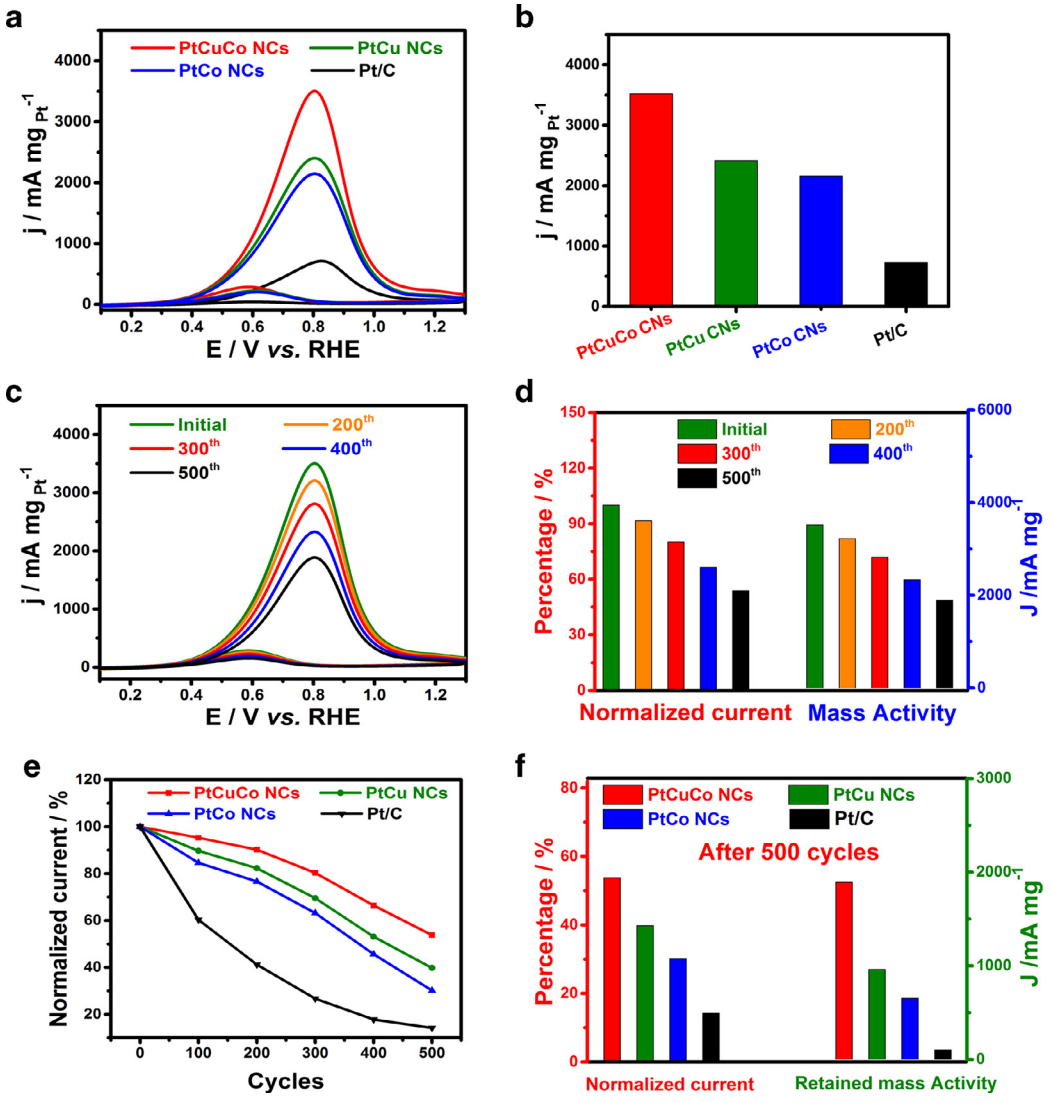

Fig. 5. (a) CV curves of PtCuCo, PtCu, and PtCo NCs, as well as Pt/C catalysts towards GOR at the scan rate of 50 mV s^{-1}. (b) The corresponding histogram of mass activities of these electrocatalysts. (c) Initial, 200th, 300th, 400th, and 500th CV curves of PtCuCo towards GOR and (d) its corresponding histogram of normalized current percentage and retained mass activities. (e) Durability comparison of PtCuCo, PtCu, and PtCo NCs, as well as Pt/C catalysts towards GOR and its corresponding histogram of normalized current percentage and retained mass activities.

carbon electrode to obtain the working electrodes. As for the electrochemical tests, the sample-coated glassy carbon electrode, a saturated calomel electrode, and a Pt wire were selected as working electrode, a reference electrode, and a counter electrode, respectively. The EGOR and GOR tests were conducted in the CHI760e electrochemical workstation in the solution of 1.0 M KOH + 1.0 M EG and 1.0 M KOH + 1.0 M glycerol at room temperature, respectively. For comparison, the commercial Pt/C (20 wt%, 2–5 nm Pt nanoparticles) purchased from Johnson Matthey (JM) Corporation was selected as the reference catalyst. The mass activities were normalized with respect to the Pt amount on the electrodes. Besides, continuous 500 cycles CVs with the reference electrode of Hg/HgO have also been conducted for evaluating their durability. The electrochemical impedance spectroscopy (EIS) has also been conducted to further study the charge transfer efficiency at the electrode and electrolyte interface.

3. Results and discussion

Experimentally, we prepared trimetallic PtCuCo NCs via a facile co-reduction method using CTAB as surfactant agents in the presence of OAm solution. The PtCuCo NCs were first characterized by TEM. As displayed in TEM images in the Fig. 1(a)–(c), the products consisted of uniform six-armed starlike NCs with a high yield over 90%. To better visualize the structure of the as-prepared products, the higher-resolution TEM images were also obtained. As seen in Fig. 1(d), most of the NCs were observed as six-armed stars with the diameter around 11.9 nm (Fig. S1), indicating the presence of hexagonal PtCuCo NCs. According to the SEM-EDX (Fig. 1(e)) and Table S1, we can infer that the atomic ratio of Pt/Cu/Co is 51.7:23.2:25.1, being consistent with the results from ICP-AES (50.9: 24.1: 25.0). Moreover, the PXRD patterns were also obtained to investigate their structures. As shown in Fig. 1(f), the PXRD patterns of PtCuCo NCs display the typical face-centered cubic (fcc) structure, well matching with the previously reported fcc Pt [32]. Remarkably, the PXRD patterns of PtCuCo showed slight shift in comparison with standard Pt, Cu, and Co, revealing the formation of alloy phase in such hexagonal PtCuCo NCs [33,34].

For comparison, PtCo and PtCu NCs were also prepared through the same method except for the introduction of $CuCl_2{\cdot}2H_2O$ and $Co(acac)_2$. The TEM was also employed to characterize their morphologies. As displayed in Fig. 2(a) and (b), some highly uniform PtCo nanoparticles with irregular shapes were obtained, and the EDX spectrum showed that the atomic ratio of Pt/Co was 75.4: 24.6

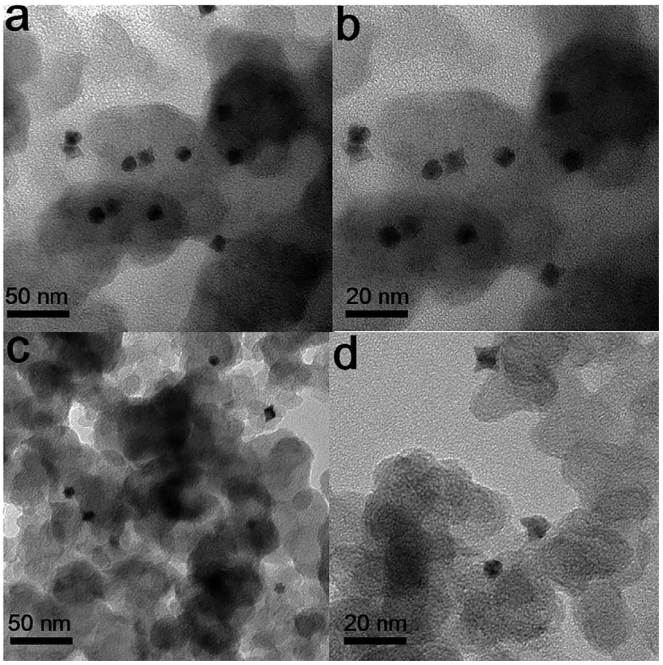

Fig. 6. Representative TEM images of carbon black supported hexagonal PtCuCo NCs (a and b) before and (c and d) after 500 cycles electrochemical tests.

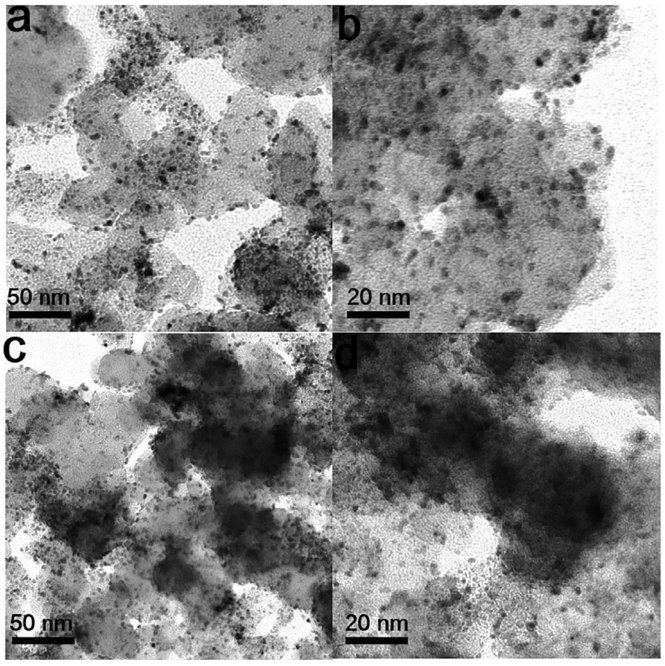

Fig. 7. Representative TEM images of commercial Pt/C catalysts (a and b) before and (c and d) after 500 cycles electrochemical tests.

(Fig. 2(c)), indicating the successful preparation of PtCo NCs. With regard to PtCu NCs, as seen in Fig. 2(d) and (e), the products consisted of many five-armed starlike nanoparticles and some small size nanocubes. Moreover, the atomic ratio of Pt/Cu was measured to be 54.2: 45.8 (Fig. 2(f)), indicating the complete reduction of $Pt(acac)_2$ and $CuCl_2{\cdot}2H_2O$. These results have suggested that both the addition of $CuCl_2{\cdot}2H_2O$ and $Co(acac)_2$ is highly significant for the successful preparation of hexagonal PtCuCo NCs.

To characterize the crystalline structures of the as-prepared PtCo and PtCu NCs, the PXRD patterns of these two types of nanostructures were also acquired. As seen in Fig. 3(a), the PXRD peaks of PtCo located between standard Pt (PDF-#87-0640) and Co (PDF-#01-1255), suggesting the formation of PtCo alloy [35]. Similarly, the PXRD peaks of PtCu located between standard Pt (PDF-#87-0640) and Cu (PDF-#04-0836), also revealing the presence of PtCu alloy in the PtCu NCs [36].

To better study the properties of the hexagonal PtCuCo NCs, we have also employed the XPS to trace their surface chemical compositions. Fig. 3(b) displays the XPS spectra of Pt 4f, it can be found that Pt 4f shows mainly the metallic state on the surface. More interestingly, compared to the pristine Pt 4f (71.0 and 74.4 eV for Pt 4f 7/2 and Pt 4f 5/2, respectively) (Fig. S2), the Pt 4f in PtCuCo NCs displayed a positive shift to the higher binding energy of 71.5 and 74.8 eV, respectively. These results suggested that the incorporation of Cu and Co into Pt greatly change the electronic structure of Pt, which is a significant factor for improving the electrocatalytic activity [37,38]. As for Cu 2p, its XPS spectra can be well deconvoluted into two sets of peaks (Cu 2p 3/2 and Cu 2p 1/2) (Fig. 3(c)). Remarkably, the results revealed that the surface Cu in PtCuCo NCs is mainly in metallic state, indicating the complete reduction of $CuCl_2$, while the presence of some weak Cu (II) peaks is ascribed to the surface oxidation of Cu species in air [39]. Fig. 3(d) showed the spectrum of Co 2p, which included two pairs of spin-orbit doublets arising from 2p 1/2 and 2p 3/2, as well as two shakeup satellites. Apart from the metallic states, the other two well fitted peaks for 2p 3/2 could be ascribed to the Co^{3+} (≈780.6 eV) and Co^{2+} (≈782.7 eV), respectively [40].

Considering the unique hexagonal shape, abundant surface active areas, as well as strengthened electronic effects, the newly generated trimetallic PtCuCo nanostructures should possess great promising for serving as high-efficiency electrocatalysts toward fuel cells reactions [41]. To this end, EGOR and GOR have been selected as the model reactions to examine the electrocatalytic performances of the engineered hexagonal PtCuCo NCs. Commercial Pt/C catalysts were also employed for comparison. Fig. 4(a) compares the CV curves for the electrooxidation of EG on different catalysts, as seen, the onset potential for PtCuCo NCs is 0.33 V, which is smaller than those of Pt/C (0.45 V), PtCu NCs (0.36 V), and PtCo NCs (0.39 V), indicating the better EG oxidation capability of PtCuCo NCs. Electroactive surface areas (ECSA) that calculated on the basis of hydrogen adsorption/desorption peaks are 48.5, 41.7, 38.6, and 54.3 $m^2\ g^{-1}$ for PtCuCo NCs, PtCu NCs, PtCo NCs, and commercial Pt/C, respectively (Fig. S3). And the higher ECSA of PtCuCo NCs thus confirmed the abundant surface active sites, which was significant for promoting their electrocatalytic performances. The mass activities of different catalysts were normalized to the masses of Pt on the surface of electrode, which have been summarized in Fig. 4(b). Remarkably, the PtCuCo NCs show the sharp peak at 0.6 V (vs RHE) in the positive scan, which is ascribed to the electroxidation of EG, while the peak in the backward (0.6 V) is associated with the removal of carbonaceous species (such as CO) produced in the forward electrooxidation scan. The mass activity of PtCuCo NCs is calculated to be 4926.4 mA mg^{-1}, which is 4.2 times greater than that of commercial Pt/C catalysts (1161.2 mA mg^{-1}). Besides the comparison with commercial Pt/C, it also shows higher electrocatalytic activity than that of some previously published works (Table S2). Moreover, benefitting from the electronic and synergistic effects between Pt and Cu (or Co), both PtCu and PtCo NCs also displayed greatly promoted electrocatalytic activity of 3479.9 and 3157.6 mA mg^{-1}, respectively. In addition, we have also examined the long-term stability of such PtCuCo NCs since the durability is an important parameter for evaluating the electrochemical properties of the catalysts [42,43], which is significant for the practical application in fuel cells. As shown in Fig. 4(c) and (d), the peak current densities of catalysts decayed rapidly over scan cycles in the initial period, being ascribed to partial poisoning or dissolution of catalysts. Regardless of these, the

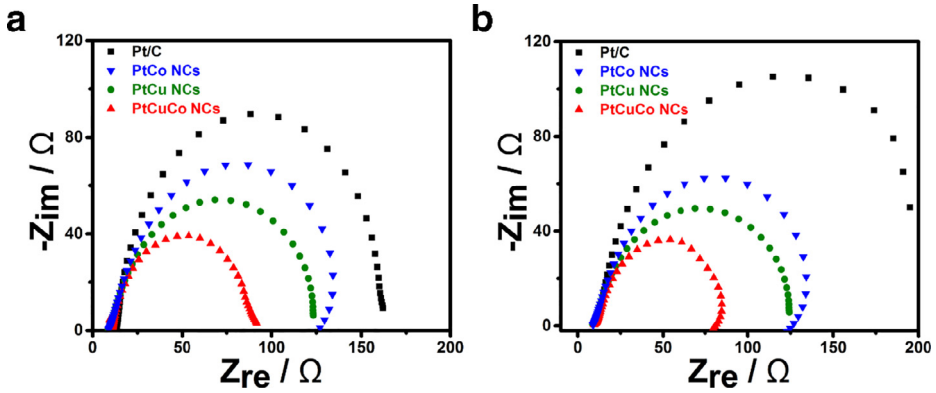

Fig. 8. Nyquists of PtCuCo, PtCu, and PtCo NCs, as well as Pt/C catalysts in (a) 1.0 M EG + 1.0 M KOH and (b) 1.0 M glycerol + 1.0 M KOH solution at the potential of 0.8 V (vs RHE).

hexagonal PtCuCo nanocatalysts can also retain high mass activity and normalized current percentage of 2740.6 mA mg^{-1} and 55.7% after continuous 500 cycles CV. For comparison, the long-term stabilities of other three types of electrocatalysts have also been examined via the successive 500 cycles CV. As seen in Fig. 4(e) and (f), the normalized current percentages of all the electrocatalysts decreased fleetly with the increasing of cycles. Among them, the hexagonal PtCuCo nanocatalysts still possess the highest retained mass activity and normalized current, which are 18.5 and 4.4 times higher than those of Pt/C catalysts, whose retained mass activity and normalized current percentage founded to be 148.6 mA mg^{-1} and 12.8%, respectively. In addition, PtCu and PtCo NCs also possessed greatly enhanced long-term stability with the retained mass activities of 1419.8 and 868.3 mA mg^{-1}, both of which were much superior to commercial Pt/C catalysts.

Besides the EGOR, the electrocatalytic performances of the as-obtained PtCuCo NCs were further studied by GOR. The CV was conducted in 1 M KOH and 1 M glycerol solution at the scan rate of 50 mV s^{-1}. Fig. 5(a) shows the CV curves of different electrocatalysts towards GOR. As seen in Fig. 5(a) and (b), similar behavior was also found in the electrooxidation of glycerol, in which the PtCuCo NCs displayed the highest peak current density of 3519.9 mA mg^{-1}, which was about 4.86, 1.63, and 1.46 times greater than those of Pt/C (723.9 mA mg^{-1}), PtCo (2160.9 mA mg^{-1}), and PtCu (2414.8 mA mg^{-1}), respectively. More importantly, we also found that the electrocatalytic activity of such PtCuCo NCs was also much higher than those of previous works (Table S3). Additionally, the successive 500 cycles CV were also conducted to study their long-term stability. As is displayed in Fig. 5(c) and (d), such PtCuCo NCs can also keep super high mass activity of 1893.7 mA mg^{-1} after 500 cycles CV, and its normalized current percentage was also measured to be 53.8%, which is much higher than that of Pt/C (14.2%), PtCo (30.3%), and PtCu nanocatalysts (39.8%) (Fig. 5(e) and (f)). Moreover, the CA tests also indicated that such hexagonal PtCuCo NCs could also display the highest retained mass activities of 746.3 and 432.5 mA mg^{-1} after 3600 s for EGOR and GOR, respectively, both of which were much higher than those of Pt/C, PtCu NCs, and PtCo NCs, further confirming the great enhancement in long-term stability (Fig. S4 and S5). After long-term electrochemical measurements, the atomic ratio of Pt/Cu/Co determined by ICP-AES was 53.6:22.4:24.0, which was almost the same with original one. Furthermore, after comparing with recently published studies, we also find that such hexagonal PtCuCo NCs possess both enhanced long-term stability toward EGOR and GOR (Table S4). These results have highlighted the superior stability towards GOR without remarkable composition, size, morphology, and structure variations after the 500 cycles CV tests, as demonstrated by TEM characterizations (Fig. 6). However, by contrast, the Pt/C catalysts faced serious aggregation during stability measurement (Fig. 7 and S6).

The EIS tests were also carried out to study the charge transfer and electrochemical reaction process, which were conducted in the 1.0 M EG + 1.0 M KOH and 1.0 M glycerol + 1.0 M KOH solutions at the potential of 0.8 V (vs RHE). As shown in Fig. 8(a), the PtCuCo NCs displayed the smallest diameter of semicircle arc (DIA) among all investigated electrocatalysts, suggesting the smallest resistance but fastest interfacial charge transport in 1.0 M EG + 1.0 M KOH solution [44]. Similar behavior could also be found in 1.0 M glycerol + 1.0 M KOH solution (Fig. 8(b)), for which PtCuCo NCs possessed the smallest DIA and best conductivity among these electrocatalysts [45]. These results clearly demonstrate that the incorporation of Cu and Co into Pt endow them with both enhanced conductivity and catalytic activity.

4. Conclusions

In general, a novel class of trimetallic PtCuCo NCs has been successfully engineered through a facile method. The presence of $CuCl_2$ and $Co(acac)_2$ in the reaction system is the key factor for the successful construction of well-defined PtCuCo NCs. The hexagonal PtCuCo nanostructures can be readily employed as highly active and durable electrocatalysts for fuel cell reactions. Impressively, the optimized PtCuCo NCs showed a great enhancement in catalytic activity for the electrooxidation of EG and glycerol, outperforming the PtCu NCs, PtCo NCs, as well as Pt/C catalysts. The enhanced activity of PtCuCo nanocatalysts is ascribed to the electronic effects as well as the unique hexagonal nanostructure. We believe that our work would provide some significant opportunities for the rational fabrication of well-defined multicomponent nanostructures with desirable functionalities for the practical applications of fuel cells and beyond.

Acknowledgments

This work was sponsored by K.C. Wong Magna Fund in Ningbo University. The authors also appreciate to the National Natural Science Foundation of China (Grant 21603111, 51702173, 41522304 and 21577142).

Supplementary materials

Supplementary material associated with this article can be found, in the online version, at doi:10.1016/j.jtice.2018.08.023.

References

[1] Becknell N, Kang Y, Chen C, Resasco J, Kornienko N, Guo J, Markovic NM, Somorjai GA, Stamenkovic VR, Yang P. Atomic structure of Pt_3Ni nanoframe electrocatalysts by in situ X-ray absorption spectroscopy. J Am Chem Soc 2015;137:15817–24.

[2] Ataee-Esfahani H, Imura M, Yamauchi Y. All-metal mesoporous nanocolloids: solution-phase synthesis of core-shell Pd@Pt nanoparticles with a designed concave surface. Angew Chem 2013;52:13611–15.

[3] Chen C, Kang Y, Huo Z, Zhu Z, Huang W, Xin HL, Snyder JD, Li D, Herron JA, Mavrikakis M, Chi M, More KL, Li Y, Markovic NM, Somorjai GA, Yang P, Stamenkovic VR. Highly crystalline multimetallic nanoframes with three-dimensional electrocatalytic surfaces. Science 2014;343:1339–43.

[4] Shen Y, Gong B, Xiao K, Wang L. In situ assembly of ultrathin PtRh nanowires to graphene eanosheets as eighly efficient electrocatalysts for the oxidation of ethanol. ACS Appl Mater Interfaces 2017;9:3535–43.

[5] Zhang H, Shang Y, Zhao J, Wang J. Enhanced electrocatalytic activity of ethanol oxidation reaction on palladium-silver nanoparticles via removable surface ligands. ACS Appl Mater Interfaces 2017;9:16635–43.

[6] Bu L, Shao Q, Bin E, Guo J, Yao J, Huang X. PtPb/PtNi intermetallic core/atomic layer shell octahedra for efficient oxygen reduction electrocatalysis. J Am Chem Soc 2017;139:9576–82.

[7] Ma Y, Yin L, Yang T, Huang Q, He M, Zhao H, Zhang D, Wang M, Tong Z. One-pot synthesis of concave platinum–cobalt nanocrystals and their superior catalytic performances for methanol electrochemical oxidation and oxygen electrochemical reduction. ACS Appl Mater Interfaces 2017;9:36164–72.

[8] Wang Q, Zhao Z, Jia Y, Wang M, Qi W, Pang Y, Yi J, Zhang Y, Li Z, Zhang Z. Unique Cu@CuPt sore-shell concave octahedron with enhanced methanol oxidation activity. ACS Appl Mater Interfaces 2017;9:36817–27.

[9] Zheng L, Yang D, Chang R, Wang C, Zhang G, Sun S. Crack-tips enriched platinum–copper superlattice nanoflakes as highly efficient anode electrocatalysts for direct methanol fuel cells. Nanoscale 2017;9:8918–24.

[10] Qazzazie D, Yurchenko O, Urban S, Kieninger J, Urban G. Platinum nanowires anchored on graphene-supported platinum nanoparticles as a highly active electrocatalyst towards glucose oxidation for fuel cell applications. Nanoscale 2017;9:6436–47.

[11] Huang L, Han Y, Zhang X, Fang Y, Dong S. One-step synthesis of ultrathin Pt_xPb nerve-like nanowires as robust catalysts for enhanced methanol electrooxidation. Nanoscale 2017;9:201–7.

[12] Fu S, Zhu C, Song J, Zhang P, Engelhard MH, Xia H, Du D, Lin Y. Low Pt-content ternary PdCuPt nanodendrites: an efficient electrocatalyst for oxygen reduction reaction. Nanoscale 2017;9:1279–84.

[13] Xu H, Yan B, Li S, Wang J, Song P, Wang C, Guo J, Du Y. Highly open bowl-like PtAuAg nanocages as robust electrocatalysts towards ethylene glycol oxidation. J Power Sources 2018;384:42–7.

[14] Du C, Gao X, Zhuang Z, Cheng C, Zheng F, Li X, Chen W. Epitaxial growth of zigzag PtAu alloy surface on Au nano-pentagrams with enhanced Pt utilization and electrocatalytic performance toward ethanol oxidation reaction. Electrochim Acta 2017;238:263–8.

[15] Lee J-E, Jang YJ, Xu W, Feng Z, Park H-Y, Kim JY, Kim DH. PtFe nanoparticles supported on electroactive Au–PANI core@shell nanoparticles for high performance bifunctional electrocatalysis. J Mater Chem A 2017;5:13692–9.

[16] Chen Q, Yang Y, Cao Z, Kuang Q, Du G, Jiang Y, Xie Z, Zheng L. Excavated cubic platinum-tin alloy nanocrystals constructed from ultrathin nanosheets with enhanced electrocatalytic activity. Angew Chem 2016;55:9021–5.

[17] Mahmood A, Xie N, Ud Din MA, Saleem F, Lin H, Wang X. Shape controlled synthesis of porous tetrametallic PtAgBiCo nanoplates as highly active and methanol-tolerant electrocatalyst for oxygen reduction reaction. Chem Sci 2017;8:4292–8.

[18] Zhai C, Hu J, Sun M, Zhu M. Two dimensional visible-light-active Pt-BiOI photoelectrocatalyst for efficient ethanol oxidation reaction in alkaline media. Appl Surf Sci 2018;430:578–84.

[19] Xu H, Yan B, Li S, Wang J, Wang C, Guo J, Du Y. Facile construction of N–doped graphene supported hollow PtAg nanodendrites as highly efficient electrocatalysts toward formic acid oxidation reaction. ACS Sustain Chem Eng 2017;6:609–17.

[20] Xu H, Yan B, Li S, Wang J, Wang C, Guo J, Du Y. N-doped graphene supported PtAu/Pt intermetallic core/dendritic shell nanocrystals for efficient electrocatalytic oxidation of formic acid. Chem Eng J 2018;334:2638–46.

[21] Weng X, Liu Q, Feng JJ, Yuan J, Wang AJ. Dendrite-like PtAg alloyed nanocrystals: Highly active and durable advanced electrocatalysts for oxygen reduction and ethylene glycol oxidation reactions. J Colloid Interface Sci 2017;504:680–7.

[22] Dutta S, Ray C, Sasmal AK, Negishi Y, Pal T. Fabrication of dog-bone shaped Au NR core-Pt/Pd shell trimetallic nanoparticle-decorated reduced graphene oxide nanosheets for excellent electrocatalysis. J Mater Chem A 2016;4:3765–76.

[23] Zhang N, Guo S, Zhu X, Guo J, Huang X. Hierarchical Pt/Pt_xPb core/shell nanowires as efficient catalysts for electrooxidation of liquid fuels. Chem Mater 2016;28:4447–52.

[24] Xu H, Wang J, Yan B, Zhang K, Li S, Wang C, Shiraishi Y, Du Y, Yang P. Hollow Au_xAg/Au core/shell nanospheres as efficient catalysts for electrooxidation of liquid fuels. Nanoscale 2017;9:12996–3003.

[25] Xu H, Wang J, Yan B, Li S, Wang C, Shiraishi Y, Yang P, Du Y. Facile construction of fascinating trimetallic PdAuAg nanocages with exceptional ethylene glycol and glycerol oxidation activity. Nanoscale 2017;9:17004–12.

[26] Bai J, Fang CL, Liu ZH, Chen Y. A one-pot gold seed-assisted synthesis of gold/platinum wire nanoassemblies and their enhanced electrocatalytic activity for the oxidation of oxalic acid. Nanoscale 2016;8:2875–80.

[27] Fu S, Zhu C, Shi Q, Xia H, Du D, Lin Y. Highly branched PtCu bimetallic alloy nanodendrites with superior electrocatalytic activities for oxygen reduction reactions. Nanoscale 2016;8:5076–81.

[28] Zhang N, Bu L, Guo S, Guo J, Huang X. Screw thread-like platinum-copper nanowires bounded with high-index facets for efficient electrocatalysis. Nano Lett 2016;16:5037–43.

[29] Bu L, Guo S, Zhang X, Shen X, Su D, Lu G, Zhu X, Yao J, Guo J, Huang X. Surface engineering of hierarchical platinum-cobalt nanowires for efficient electrocatalysis. Nature Commun 2016;7:11850.

[30] Xu H, Yan B, Zhang K, Wang J, Li S, Wang C, Shiraishi Y, Du Y, Yang P. Eco-friendly and facile synthesis of novel bayberry-like PtRu alloy as efficient catalysts for ethylene glycol electrooxidation. Int J Hydrogen Energy 2017;42:20720–8.

[31] Xu H, Liu C, Song P, Wang J, Gao F, Zhang Y, Shiraishi Y, Di J, Du Y. Achieving remarkable performances towards ethylene glycol electrooxidation based on pentangle-like PtCu nanocatalysts. Chem Asian J 2018;13:626–30.

[32] Gan QM, Tao L, Zhou LN, Zhang XT, Wang S, Li YJ. Directional coalescence growth of ultralong $Au_{93}Pt_7$ alloy nanowires and their superior electrocatalytic performance in ethanol oxidation. Chem Commun 2016;52:5164–6.

[33] Hong W, Shang C, Wang J, Wang E. Trimetallic PtCuCo hollow nanospheres with a dendritic shell for enhanced electrocatalytic activity toward ethylene glycol electrooxidation. Nanoscale 2015;7:9985–9.

[34] Liu L, Samjeské G, Takao S, Nagasawa K, Iwasawa Y. Fabrication of PtCu and PtNiCu multi-nanorods with enhanced catalytic oxygen reduction activities. J Power Sources 2014;253:1–8.

[35] Luo W, Baaziz W, Cao Q, Ba H, Baati R, Ersen O, Pham-Huu C, Zafeiratos S. Design and fabrication of highly reducible PtCo rarticles supported on graphene–coated ZnO. ACS Appl Mater Interfaces 2017;9:34256–68.

[36] Li H-H, Fu Q-Q, Xu L, Ma S-Y, Zheng Y-R, Liu X-J, Yu S-H. Highly crystalline PtCu nanotubes with three dimensional molecular accessible and restructured surface for efficient catalysis. Energy Environ Sci 2017;10:1751–6.

[37] Zhang Z-C, Tian X-C, Zhang B-W, Huang L, Zhu F-C, Qu X-M, Liu L, Liu S, Jiang Y-X, Sun S-G. Engineering phase and surface composition of Pt_3Co nanocatalysts: A strategy for enhancing CO tolerance. Nano Energy 2017;34:224–32.

[38] Beermann V, Gocyla M, Kuhl S, Padgett E, Schmies H, Goerlin M, Erini N, Shviro M, Heggen M, Dunin-Borkowski RE, Muller DA, Strasser P. Tuning the electrocatalytic oxygen reduction reaction activity and stability of shape-controlled Pt-Ni nanoparticles by thermal annealing – elucidating the surface atomic structural and compositional changes. J Am Chem Soc 2017;139:16536–47.

[39] Xu H, Yan B, Wang J, Zhang K, Li S, Xiong Z, Wang C, Shiraishi Y, Du Y, Yang P. Self-supported porous 2D AuCu triangular nanoprisms as model electrocatalysts for ethylene glycol and glycerol oxidation. J Mater Chem A 2017;5:15932–9.

[40] Ma X, Zhang W, Deng Y, Zhong C, Hu W, Han X. Phase and composition controlled synthesis of cobalt sulfide hollow nanospheres for electrocatalytic water splitting. Nanoscale 2018;10:4816–24.

[41] Zhou LN, Zhang XT, Wang ZH, Guo S, Li YJ. Cubic superstructures composed of PtPd alloy nanocubes and their enhanced electrocatalysis for methanol oxidation. Chem Commun 2016;52:12737–40.

[42] Yang Z-Z, Liu L, Wang A-J, Yuan J, Feng J-J, Xu Q-Q. Simple wet-chemical strategy for large-scaled synthesis of snowflake-like PdAu alloy nanostructures as effective electrocatalysts of ethanol and ethylene glycol oxidation. Int J Hydrogen Energy 2017;42:2034–44.

[43] Han S-H, Ji Y-G, Xing S-H, Hui J-J, Guo Q, Shi F, Chen P, Chen Y. Carbon nanotubes supported platinum–gold alloy nanocrystals composites with ultrahigh activity for the formic acid oxidation reaction. Int J Hydrogen Energy 2017;42:2096–103.

[44] Zhu M, Zhai C, Sun M, Hu Y, Yan B, Du Y. Ultrathin graphitic C_3N_4 nanosheet as a promising visible-light-activated support for boosting photoelectrocatalytic methanol oxidation. Appl Catal Environ 2017;203:108–15.

[45] Xu H, Yan B, Zhang K, Wang C, Zhong J, Li S, Du Y, Yang P. PVP-stabilized PdAu nanowire networks prepared in different solvents endowed with high electrocatalytic activities for the oxidation of ethylene glycol and isopropanol. Colloids Surf A 2017;522:335–45.